Cleaner Materials 15 (2025) 100287

Contents lists available at ScienceDirect

Cleaner Materials

journal homepage: www.journals.elsevier.com/cleaner-materials

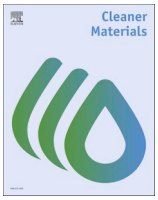

Functionalized biochar from vegetable waste for phosphorus removal from aqueous solution and its potential use as a slow-release fertilizer

Rajesh Chanda [a,*], Toslim Jahid [a], Anik Karmokar [a], Bejoy Hossain [a], Md. Moktadir [a], Md. Saiful Islam [b], Nirupam Aich [c], Biplob Kumar Biswas [a,*]

[a] Department of Chemical Engineering, Jashore University of Science and Technology, Jashore 7408, Bangladesh
[b] Department of Nanomaterials and Ceramics Engineering, Bangladesh University of Engineering Technology, Dhaka 1000, Bangladesh
[c] Department of Civil and Environmental Engineering, University of Nebraska-Lincoln, Nebraska Hall W181, 900 N 16th St, Lincoln, NE, USA

ARTICLE INFO

Keywords:
Metal chloride-doped Biochar
Adsorption
Kinetics
Slow-release fertilizer
Circular economy

ABSTRACT

Agricultural runoff of phosphorus leads to the loss of this critical nutrient into the waterbodies and causes environmental problems like eutrophication. To tackle the growing concern, functionalized biochar as an adsorbent provides a sustainable method to capture the phosphorus from wastewater. Additionally, the P-laden biochar as a slow-release fertilizer improves plant nutrient uptake and crop yield. In this work, metal chloride-doped biochar derived from non-edible vegetable waste was prepared and applied as an adsorbent. Zinc chloride-doped biochar (ZBC) showed a better phosphorus adsorption capacity of 47.83 mg/g among the prepared biochar. The desorption study suggested that around 42 % of total adsorbed P was released within 336 h. The growth of mung plants over 70 days was monitored, along with mung bean yield, to assess the effectiveness of P-laden ZBC as a slow-release phosphorus fertilizer. The presented approach of non-edible waste valorization into slow-release fertilizer could contribute to tackling nutrient depletion and achieving a circular economy.

1. Introduction

Phosphorus (P) is a crucial nutrient for crop production, being a key component of NPK fertilizer and a non-renewable resource. To date, mineral phosphate rock, a non-renewable resource, is the primary source of phosphorus-based fertilizer worldwide. Approximately 20 M tons of P as a mineral are extracted from the Earth each year (Weferling et al., 2016). According to the Argus Consulting Services report for the International Fertilizer Association in 2023, the natural phosphorus supply could be depleted within the next 175–400 years (Argus Consulting Services, 2023). Recognizing the importance of phosphorus into consideration, the EU labeled phosphate rock and white phosphorus as critical raw materials in 2020 (Santos et al., 2021). However, a mere 16 % of the applied phosphorus as fertilizer is utilized during typical crop production. The unutilized phosphorus is lost through soil erosion, crop residues, and a significant portion of runoff in the nearby aquatic reservoirs, creating the risk of eutrophication (Jupp et al., 2021). Therefore, the dwindling supply of phosphorus and the environmental concerns associated with phosphorus in surface waters have underscored the need for phosphorus recovery and recycling.

Among the water sources, wastewater streams (untreated stream, urine, etc.), animal manure, municipal sludge, and sewage sludge ash possess the highest phosphorous recovery potential (Witek-Krowiak et al., 2022). According to the Danish Environmental Agency, around 20 % of the total imported phosphorus in Denmark can be met by reusing phosphorus from wastewater (Christensen et al., 2022). Several processes, like struvite formation, electrochemical precipitation, enhanced biological phosphorus recovery (EBPR), membrane filtration, adsorption, etc., are applied for phosphorous recovery (Witek-Krowiak et al., 2022). Among them, struvite, a salt containing magnesium, ammonium, and phosphate, gained the most interest due to its potential use as a slow-release fertilizer (Lin et al., 2024). However, only 40 % of the P in wastewater treatment plants can be removed by this technique (Ghosh et al., 2019). The electrochemical precipitation technique needs almost no external energy but has low phosphorus recovery potential (Lin et al., 2024). The membrane filtration method has high phosphorus recovery potential; however, cake layer formation, salt crystallization, and organic fouling are significant drawbacks to commercial utilization (Li et al., 2021). Adsorption is a widely studied process to remove or capture phosphorous from less concentrated sources like wastewater. It is

* Corresponding authors.
E-mail addresses: rajesh.che@just.edu.bd (R. Chanda), bk.biswas@just.edu.bd (B.K. Biswas).

https://doi.org/10.1016/j.clema.2024.100287
Received 27 July 2024; Received in revised form 12 December 2024; Accepted 13 December 2024
Available online 16 December 2024

noteworthy that orthophosphate ($H_2PO_4^-$, HPO_4^{2-}, and PO_4^{3-}) is the most dominating phosphorous species in the domestic wastewater stream (Jupp et al., 2021). Therefore, the recovery of phosphorus from wastewater using adsorbent is focused on orthophosphate recovery and removal.

Among the various adsorbent materials, renewable bio-based materials are essential in implementing a sustainable circular economy. The growing global population and urbanization lead to higher resource consumption and an increasing waste generation rate. The incremental waste consequently puts pressure on environmental sustainability. Therefore, the concept of a "circular economy" is becoming essential to tackle the increasing resource demand and minimize negative environmental impacts. According to the United States Environmental Protection Agency (EPA), waste recapture as a resource to produce/manufacture new materials and products is one of the main backbones of the circular economy. As a part of the circular economy plan set by the European Commission in May 2023, 65 % of the waste materials have to be reused, and the amount of waste material for landfilling will be reduced to less than 10 % of total waste by 2030 (Commission, 2023). Every year, around 200 billion tons of agricultural residues are generated worldwide (Kamusoko et al., 2021). Therefore, to implement a circular economy, it is necessary to find ways to create valuable products using agro-based wastes.

Non-edible parts of vegetables are one of the major portions of agricultural residues. This lignocellulosic residue can be converted into valuable products such as biofuel, bioplastic, biopolymers, etc., by applying diversified techniques (Capanoglu et al., 2022). Pyrolysis of such agricultural residues produces biochar, a sustainable method for producing multi-functional material due to its porous carbonaceous structure and the inherent presence of various functional groups (Sun et al., 2020). The type of feedstock influences biochar functionality. It plays a key role in its applicability as an adsorbent for capturing heavy metals, acting as a catalyst (Sun et al., 2020), enhancing carbon sequestration (Feng et al., 2020), and improving soil quality to increase crop productivity (Pal et al., 2021). Biochar can be easily functionalized with different metal cations by co-pyrolysis and post-modification with ligands to improve the applicational performance such as enhancing heavy metal, nutrients, and wastewater remediation (Chanda et al., 2024; Yang et al., 2020). Biochar derived from various feedstocks like wood, corncobs, rice husks, sawdust (Kizito et al., 2017), cacao shells, and corn cobs (Hale et al., 2013), etc. were reported for the removal of phosphorus. The phosphate adsorption by biochar depends on its mineral percentage and surface properties (Samaraweera et al., 2023). The pristine biochar contains an oxygenated functional group and minimum cation content, which binds with cations and results in poor phosphate adsorption capacity. The primary limitation of raw biochar is its low phosphorus adsorption capacity, which necessitates modification to improve phosphate adsorption and recovery (Jin et al., 2024). The pre- or post-treatment of biochar with metal salts is reported to be one of the most effective methods to improve phosphorus recovery efficiency (Jellali et al., 2023). Therefore, to enhance the performance of biochar, functionalization with metal oxides such as $MgCl_2$-modified corn straw in swine wastewater (Yu et al., 2020), $FeCl_3$-modified corn straw in biogas slurry solution (He et al., 2017), CaO-MgO added dolomite-sawdust in industrial wastewater (Li et al., 2018), waste marble powder-derived Ca-rich biochar in CSTR (Jellali et al., 2024) were utilized for phosphorus recovery. Functionalized biochar after phosphorus capture poses the potential to act as a slow-release fertilizer. The desorption of phosphorus from P-laden biochar over a broad period allows plants to utilize the available phosphorus more efficiently. Therefore, a systematic approach to non-edible vegetable waste-derived functionalized biochar for phosphorus recovery from wastewater systems and use as slow-release fertilizer is still lacking. Apart from that, raw biochar shows inconsistent performance and cannot often retain essential nutrients effectively, leading to suboptimal agricultural outcomes. By addressing these limitations and providing valuable insights, the current work has the potential to advance biochar research and its application (specifically through enhanced nutrient retention and better integration into agricultural practices), thereby paving the way for more effective and sustainable methods.

For this purpose, non-edible and discarded vegetable waste was collected from the domestic kitchen. The collected waste was then converted into biochar termed pristine biochar (PBC) or co-pyrolyzed with magnesium chloride, termed magnesium biochar (MBC), or with zinc chloride, termed zinc biochar (ZBC). Magnesium chloride was chosen as a common metal ion modification technique for biochar, where zinc chloride was selected as zinc is a crucial nutrient for healthy plants (Dhaliwal et al., 2023). However, the impact of the released zinc from ZBC into the soil was beyond the scope of this work. At temperatures below 400 °C, $ZnCl_2$ doping results in an imperfect pore structure in biochar. Conversely, temperature above 800 °C causes carbon sintering, which reduces pore area and pore volume (Zhang et al., 2024). Therefore, an appropriate ratio of $ZnCl_2$ and biochar can yield a microporous structure for carbonaceous material at an optimal carbonization temperature. Consequently, using the in-situ integration method, $ZnCl_2$ can be doped into carbonaceous material to produce ample microporous biochar after pyrolysis. From this context, the objectives of the work were to (1) prepare functional biochar from vegetable waste and to dope metal chloride by co-pyrolysis method in a limited oxygen condition, (2) study phosphate adsorption parameters, (3) perceive possible phosphate-adsorbent interactions, (4) investigate the slow-release pattern of phosphate from P-laden biochar, and (5) exploit utility of P-laden biochar as a slow-release fertilizer. The novelty of this research lies in the innovative combination of raw materials and modifiers (doping agents), along with the unique preparation methods employed to enhance P-laden biochar's effectiveness as a controlled nutrient-release agent in agricultural systems. By integrating specific organic waste sources and tailored amendments, the study develops a biochar with optimized nutrient retention and release characteristics that promote sustainable agricultural practices, setting it apart from existing approaches. The comparative adsorption studies of the prepared biochar, along with the corresponding characterization results, highlight two key findings: (1) the necessity of doping to maximize sorption capacity, and (2) the potential for using biochar derived from bio-based wastes as an effective slow-release fertilizer.

2. Materials and methods

2.1. Chemicals

Zinc chloride dihydrate (≥98 % purity, Qualikems), Magnesium chloride anhydrous (≥ 98 % purity, Merck), Sodium phosphate dibasic (98.5 %, Sigma-Aldrich), L-ascorbic acid (99 %, Smartlab), Ammonium molybdate tetrahydrate (81–83 wt% MoO_3, Sigma-Aldrich), Sodium salicylate (98 %, ResearchLab), Ammonium chloride (98 %, Merck), and HCl (37 %, Merck) were used for experimental studies. Commercial triple super phosphate (TSP) and Potash fertilizer were purchased from the local market in Jashore, Bangladesh.

2.2. Biochar preparation

The non-edible part of vegetable waste, which consists of an equal weight percentage of cauliflower stem, pineapple peel, pumpkin peel, and banana peel, was collected from local markets and domestic households. At first, the accumulated waste was rinsed with sufficient water to remove dirt. Then, the dirt-free waste was chopped into 3–4 cm sizes and oven-dried at 80 °C for 16 h. Based on a previous study, 4 g of dried material and 2 g of Zinc chloride hydrate or Magnesium chloride anhydrous were then put into a 100 ml DI water into a 250 ml beaker and stirred for 24 h (in case of pristine biochar preparation the dried vegetables waste was stirred in 100 ml DI water) (Zhang et al., 2024). Afterward, the material was collected via filtration and air-dried at room

temperature. From the collected material, 5 g was then placed into a 50 ml ceramic crucible (100 % filling) and covered with a ceramic lid. The filled crucible was then transferred into a muffle furnace and pyrolyzed at 450 °C for four hours; a heating rate of 10 K/min was used to reach the final pyrolysis temperature. After the pyrolysis, around 2 g of prepared biochar (having a yield of 40 % with respect to dried biomass) was collected, and size reduction was carried out using a mortar pestle.

2.3. Characterization

The crystalline elements of the prepared biochar were analyzed by X-ray diffraction using an Empyrean diffractometer (Malvern Panalytical) in the 2θ range of 5–80°. The scanning electron microscopy images were taken by Carl Zeiss GeminiSEM 500 microscope at a voltage of 5 kV, and energy-dispersive spectroscopy spectra of the elemental analysis of prepared biochar were measured. The X-ray Photoelectron Spectrometer (K-Alpha) was used to analyze the state of surface elements of P-laden biochar. An Al K-Alpha monochromatic X-ray source (at 1486.68 eV) was used at 15 kV and 10 mA for the survey scan and core-level spectra.

2.4. Adsorption experiment

The batch-wise adsorption experiments were carried out at room temperature using 0.5–3 g/L adsorbent dose and 20 ml synthetic solution of 100–300 mg/L concentrations of P-PO_4^{3-} using Na_2HPO_4 as the phosphate source. In a typical experiment, 20 ml of phosphate solution with biochar was poured into 250 ml conical flasks and placed into a horizontal shaker operating at 200 rpm. After the required time based on the experimental requirement (commonly after 120 min), the samples were collected via centrifugation. The removal capacity was calculated as per Eq. (1). The quantity of P-PO_4^{3-} was calculated using the molybdenum blue method (Chanda et al., 2023) and a UV–Vis spectrometer at 832 nm wavelength and adsorption capacity (q_t) was calculated using Eq. (2). The reproducibility of all the experiments conducted in this study was confirmed by repeating the tests at least twice.

$$Removal(\%) = \frac{C_o - C_t}{C_o} \times 100 \tag{1}$$

$$Adsorption\ capacity, q_t = \frac{(C_o - C_t)V}{m} \tag{2}$$

where C_t and C_0 are the final and initial phosphate concentrations in mg/L, respectively, m is the mass of the adsorbent in g, and V is the total amount of the solution in L.

2.5. Kinetics and isotherm studies

For kinetic studies, phosphate was adsorbed by $ZnCl_2$-doped biochar (ZBC) from phosphate solutions (100 mg/L and 160 mg/L) at varying contact times. The obtained data set was analyzed by two different kinetic models, namely, the pseudo-first-order (Eq.3) and pseudo-second-order model (Eq.4), and the kinetic parameters were assessed. The kinetic models can be equated sequentially as follows. (Sinha et al., 2022):

$$q_t = q_e\left(1 - e^{-k_1 t}\right) \tag{3}$$

$$q_t = \frac{k_2 q_e^2 t}{1 + k_2 q_e t} \tag{4}$$

where q_t (mg/g) signifies the adsorbed amount of phosphate at time t (min); q_e (mg/g) indicates the adsorbed phosphate at equilibrium condition; while k_1 (1/min), k_2 (g/(mg·min)) stand for the pseudo-first order and pseudo-second order adsorption rate constants, respectively.

In addition to kinetic studies, phosphate adsorption by zinc chloride-doped biochar (ZBC) was analyzed with two-parameter isotherm models such as Langmuir, Freundlich, and Temkin isotherm (Eq. 5–7). The representing equations of the itherm models, respectively, are as follows (Ayawei et al., 2017):

$$q_e = \frac{k_L q_m C_e}{1 + k_L C_e} \tag{5}$$

$$q_e = k_F C_e^{1/n} \tag{6}$$

$$q_e = \frac{RT}{b_T} \ln k_T C_e \tag{7}$$

In the equations mentioned above, q_e is the adsorption capacity at equilibrium (mg/g); C_e indicates the equilibrium concentration (mg/L); q_m designates the maximum adsorption capacity (mg/g); R is the gas constant; T is the absolute temperature (K). The other parameters are different isotherm constants that can be determined through regression analysis. Out of the remaining parameters, $1/n$ represents the adsorption intensity; b_T is the Temkin constant (J/m); k_L, k_F, and k_T indicate the Langmuir model constant related to the energy of adsorption (L/mg); Freundlich model constant incorporating all factors affecting the adsorption process. $\left(\frac{mg}{g}\left(1-\frac{1}{n}\right)^{\frac{1}{n}}\right)$, and Temkin model constant (L/mg), respectively.

2.6. Slow-release of adsorbed P and plant-based study

The slow-release studies were conducted using several 250 ml beakers. In each beaker, 100 ml of deionized water with 200 mg of P-laden ZBC was added and left without stirring. After the targeted time, the solid ZBC was separated from the remaining solution by centrifugation at 8000 rpm for 15 min. The release percentage was calculated by taking the adsorption capacity of the ZBC as the basis. Mung plant, a seasonal crop having harvesting time between November and January, was selected for plant study. The study was performed by creating three categories of same-sized plant pots: (I) control (only soil), (II) triple super phosphate (TSP) (with soil), and (III) phosphorus-adsorbed biochar (with soil). Each experimental pot (around 13 cm radius) contained 2100 g of soil. In the case of plant-pot (II) and (III), 50 mg of phosphorus equivalent/kg-soil (TSP in granule and P-laden biochar in powder form) was mixed. Since P-laden biochar is rich in phosphorus, it was necessary to use a phosphorus-rich commercial fertilizer for comparison. Therefore, TSP, a phosphorus-based commercial fertilizer, was chosen for mixing with soil in this study. This allowed a meaningful evaluation of seed germination, plant growth, and plant yield between the P-laden biochar and the P-rich commercial fertilizer. The soil was collected from agricultural fields with a soil pH of 6.8 and soil organic compound (SOC) of 2.9 %. Mung seed beans were collected from the local market. The seed beans were inserted into a 3-inch soil depth after soaking in water for 30 min. After 15 days, a 60 mg-K/kg-soil equivalent amount of potash fertilizer was given into every categorized pot after dissolving the potash fertilizer with water. After 35 days, the length of the mung plant was measured, and using a random selection method, four plants from each category were uprooted to calculate the average dry biomass. After 70 days, all the remaining plants were uprooted to collect the mung beans from the mung pods.

3. Results and discussion

3.1. Textural analysis of prepared biochar

The XRD analysis of Pristine biochar (PBC), Magnesium chloride-doped biochar (MBC), and Zinc chloride-doped biochar (ZBC) is shown in Fig. 1(a). The pristine biochar (PBC) shows the most

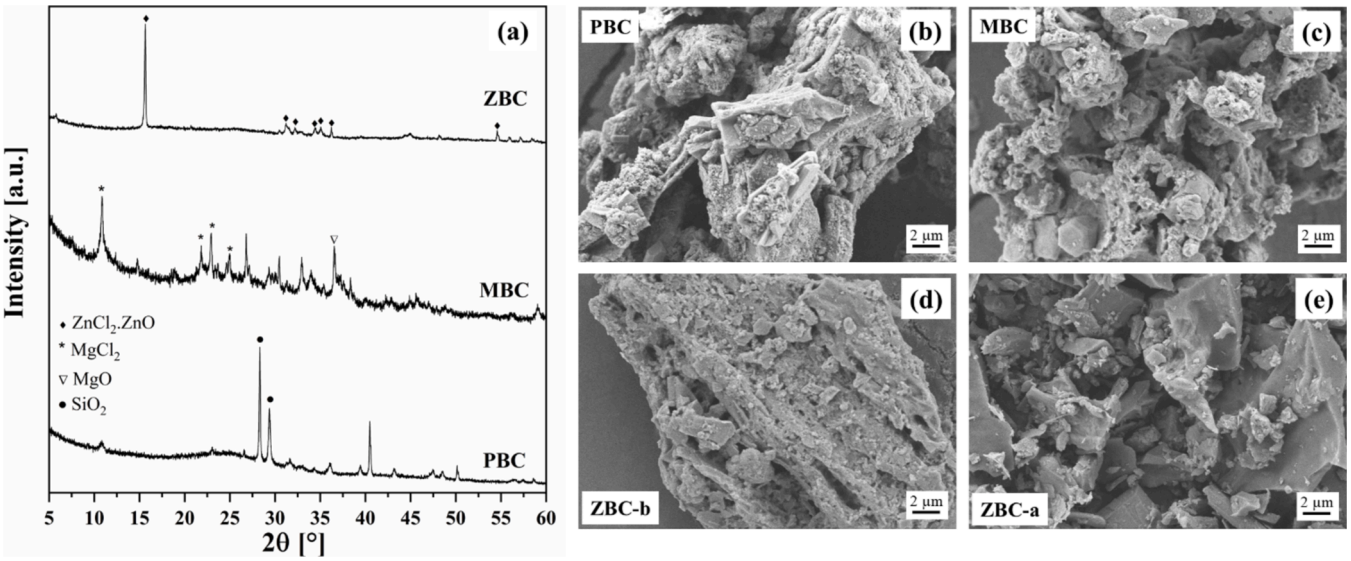

Fig. 1. Synthesized biochar's (a) XRD patterns and SEM images of (b) Pristine biochar, (c) Magnesium chloride-doped biochar, (d) Zinc chloride-doped biochar before P adsorption, (e) ZBC after P adsorption.

dominating peaks at 28.3° and 29.4°, which can be attributed to the presence of SiO_2 (JCPDS No. 41-1413) (Chen et al., 2020). The zinc-doped biochar (ZBC) shows the most intensified peak at 15.5° with minor peaks at 31.3°, 32.3°, 35.1°, 36.2° and 54.7°. All these peaks indicate the formation of $ZnO.ZnCl_2{\cdot}2H_2O$ phase (JCPDS No. 01-077-2311), which emphasizes that the transformation of $ZnCl_2$ to ZnO was not complete (Moezzi et al., 2016). This may be attributed to the fact that at temperatures above 400 °C, $ZnCl_2$ vaporizes and is partially oxidized to ZnO (Jones et al., 2013). A similar phenomenon was observed for XRD patterns of magnesium chloride co-pyrolyzed biochar (MBC). The peak at 10.9°, 21.8°, 22.9°, and 26.7° belongs to $MgCl_2$, which indicates incomplete transformation, whereas the peak at 36.7° belongs to MgO (Zhang et al., 2014). In both ZBC and MBC, the peaks corresponding to SiO_2 were absent. This was probably due to the metal chloride-based aqueous solution used during the functionalization and subsequent DI water-washing procedure.

The SEM images of pristine biochar (PBC), along with MBC and ZBC before and after phosphate adsorption, are shown in Fig. 1 (b-e). The dispersed particles on the biochar surface are visible for all the prepared ones. The size of the several biochar particles was around 40–50 μm, and the surface was rougher. In the case of both MBC and ZBC, biochar's tiny pores are also visible (Fig. 1 (b)-(c)). The EDS analysis of P-laden ZBC shows 8.9 wt% of Zn on ZBC was present (Fig. S1). Thus, it indicates that the functionalization process deposits functional metals on the surface.

3.2. *Effect of solution pH and adsorbent dosage on phosphate removal*

The initial pH of the solution is a significant dominating factor for the adsorption process of phosphate from aqueous media because of its effect on the surface charge of biochar (Khandaker et al., 2017). The solution pH is also important because it affects the structural stability of the adsorbent. The dependence of pH on the phosphate adsorption was investigated (from pH 3 to pH 9), and the result has been depicted in Fig. 2 (a). This figure exhibits that the initial pH of the solution strongly influenced phosphate adsorption on biochar. The adsorption capacity of phosphate increases from 20.59 mg/g to 41.46 mg/g with an increase in initial pH (from pH 3 to pH 5). The highest uptake capacity at the given conditions was observed at pH 5, after which the capacity decreased. From the distribution of phosphate species, it is evident that three different ionic species ($H_2PO_4^-$, HPO_4^{2-}, and PO_4^{3-}) exist in solution at various pH conditions (Chen et al., 2021). In this study, the maximum adsorption occurs as a monovalent phosphate ion ($H_2PO_4^-$), as it is the

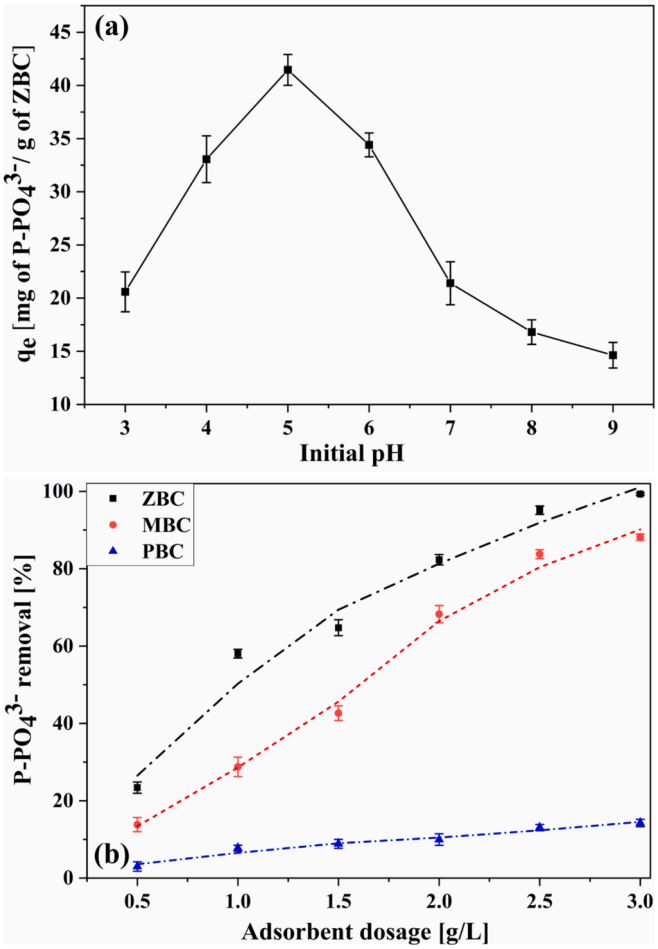

Fig. 2. (a) Effect of pH on phosphate removal using Zn-doped biochar [Condition: Initial phosphate concentration 200 mg/L; Adsorbent dosage 3.5 g/L; Shaking speed 200 rpm; Operating time 2 h], and (b) Phosphate removal using different biochar at varying doses of adsorbent. [Condition: Initial phosphate concentration 160 mg/L; pH 5; Shaking speed 200 rpm; Operating time 2 h; Room temperature].

predominating species at pH 5 (Chanda et al., 2023; Chen et al., 2021). The pH_{pzc} of the ZBC was determined to be 8.6 by the pH drift method. It signifies that the surface of the biochar is positively charged below pH 8.6 (Fig. S2). Therefore, the adsorption of existing phosphate anions was favored at a pH lower than the pH_{pzc}. However, at pH 2, the P exists predominantly as H_3PO_4, which is less favorable for adsorption onto the sites (Kumar et al., 2010). At pH 3, both H_3PO_4 and $H_2PO_4^-$ are present, leading to low adsorption at lower pH levels. At higher pH levels (6–8), the reduced adsorption capacity can be attributed to competition between anionic phosphate and hydroxyl ions for adsorption sites. However, pH 5 was selected for subsequent adsorption experiments to understand the overall adsorption scenario better.

Adsorbent dosage is a crucial parameter in adsorption studies because it defines the utilization of the optimum amount of adsorbent. In the present study, the effect of adsorbent dosage on phosphate adsorption was carried out using three different adsorbents, namely, pristine biochar (PBC), Mg-doped biochar (MBC), and Zn-doped biochar (ZBC) keeping pH, initial phosphate concentration and operating temperature constant. The influence of adsorbent dosage on phosphate removal was performed in a wide range of dosages (0.5 g/L to 3.5 g/L). The results are depicted in Fig. 2 (b), where it was obvious that the pristine biochar had the least removal capacity (16.56 % only) for all tested dosages. On the other hand, although ZBC and MBC showed similar trends in adsorption, ZBC demonstrated much better removal capacity. Since the experimental results indicated that ZBC demonstrated more pronounced effects in phosphate removal, ZBC alone was selected for performing subsequent experiments. It was evident from Fig. 2(b) that the removal of phosphate increased with the increase in adsorbent dosage. However, in the case of ZBC, complete (>99 %) removal of phosphate was achieved at an adsorbent dose of 3.0 g/L or higher.

3.3. Effect of contact time and study of sorption kinetics

Phosphate adsorption onto ZBC was conducted at different initial concentrations (100 mg/L and 160 mg/L) over varying contact times, as illustrated in Fig. 3. The adsorption capacity of ZBC adsorbent was determined to be 29 mg/g and 35 mg/g at initial concentrations of 100 mg/L and 160 mg/L, respectively. The higher uptake at the higher initial phosphate concentration can be attributed to the substantial concentration gradient between the bulk solution and adsorbent phase. It is evident from Fig. 3 that the phosphate adsorption occurred rapidly during the initial stage (up to 60 min), whereas the adsorption slowed down until equilibrium was attained. The rapid adsorption phenomenon at the initial phase can be explained by the dynamic adsorption gradient of phosphate ions moving towards the active sites of ZBC adsorbent, where ample vacant sites are readily available on the adsorbent surface.

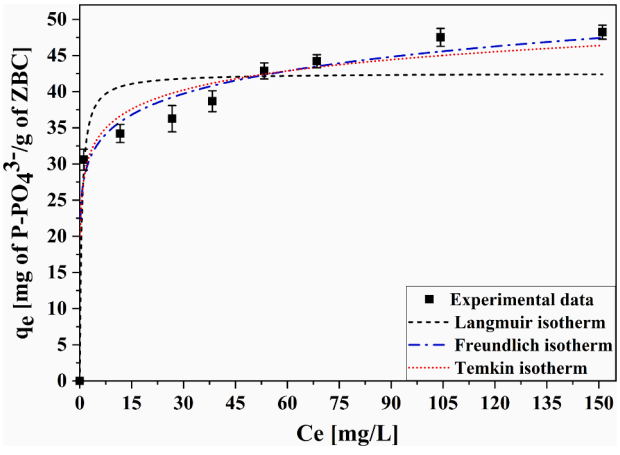

Fig. 3. Adsorption kinetics for phosphate removal onto ZBC. [Condition: Adsorbent dosage 3 g/L; pH 5; Shaking speed 200 rpm; Room temperature].

The dynamic adsorption gradient at the initial rapid adsorption phase is more significant than that at the latter phase of the sorption process. The diminution in adsorption over time can be related to an increased occupancy of the phosphate ions in the aqueous solution.

The time-bound experimental data were analyzed using pseudo-first-order and pseudo-second-order models, and the kinetic data were calculated. Fig. 3 depicts the non-linear fitting of these kinetic models along with the experimental data. The kinetic parameters of the above-described models were determined and tabulated in Table 1. Based on the coefficient of determination (R^2), the pseudo-second-order model demonstrated a better fit. This model is based on assumptions such as sorption occurring at localized sites, no interactions between sorbed ions, and the formation of a saturated monolayer on the adsorbent surface. The pseudo-second-order model contributes to explaining the process of chemisorption. These findings are consistent with previously published data (Phuong Tran et al., 2021). Therefore, it can be concluded that the adsorption adhered to a pseudo-second-order kinetic model, with sorption taking place on the localized active sites and no interaction among the adsorbed phosphate anions.

3.4. Sorption isotherms

Isotherms of phosphate adsorption by ZBC were analyzed by using Langmuir, Freundlich, and Temkin models. These models are called two-parameter equations, and it is a common practice to use two-parameter equations rather than three-parameter equations (e.g., Redlich-Peterson model) because of the inconvenience of evaluating three isotherm parameters (Zeng et al., 2004). The results of the phosphate sorption isotherm are depicted in Fig. 4, where the adsorption capacity is plotted against the equilibrium phosphate concentration. Fig. 4 indicated that the sorption capacity increases with increasing phosphate concentration at a lower concentration range, and a plateau was formed at the end. The experimental data clearly showed a characteristic L-shaped curve, where the slope remained relatively consistent at low equilibrium phosphate concentrations. In the present study, the experimental isotherm data were analyzed by fitting them to three models (Langmuir, Freundlich, and Temkin models) using the non-linear regression method. The essential parameters of the mentioned models are tabulated in Table 2. Considering the R^2 value, the Freundlich and Temkin models exhibited significantly better fitting than the Langmuir model. Based on the current experimental data, the ranking of applicability for two-parameter isotherm models is roughly as follows: Freundlich ≈ Temkin > Langmuir. The exponent $1/n$ in the Freundlich model reflects the favorability of the sorption process. A value of $1/n$ between 0.1 and 1 suggests favorable adsorption. In this study, the obtained $1/n$ value was 0.111, indicating that the adsorbent (ZBC) surface was favorable for adsorption. It also suggested a chemisorptive type of adsorption. This agrees with the study where adsorbate removal using vesicular basalt rock adsorbent was reported (Alemu et al., 2019). Nonetheless, a significantly high adsorption capacity of 47.83 mg/g was found, demonstrating that ZBC could be effectively used as an adsorbent for removing phosphate from the aqueous solutions.

The notable sorption capacity of ZBC may be attributed to the co-

Table 1
Kinetic parameters of phosphate adsorption by ZBC.

Kinetic model	Parameters	Phosphate concentration	
		100 mg/L	160 mg/L
Pseudo-first-order	k_1 (1/min)	0.17	0.16
	q_e (mg/g)	29.55	34.79
	R^2	0.98	0.99
	MAPE	4.65	2.63
Pseudo-second-order	k_2 (g/(mg·min))	0.11	0.01
	q_e (mg/g)	31.18	36.53
	R^2	0.99	0.99
	MAPE	3.40	1.70

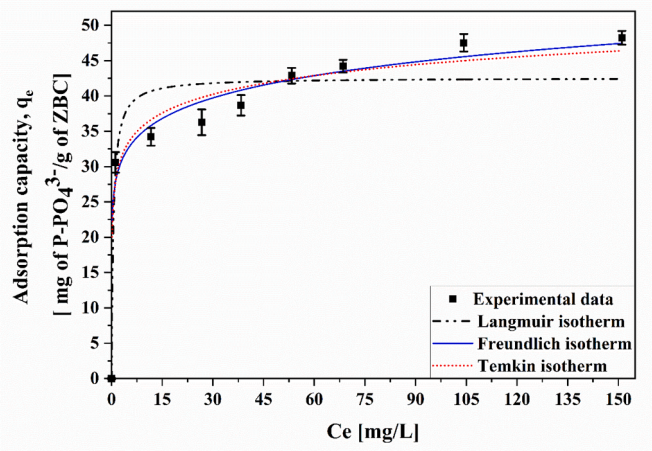

Fig. 4. Adsorption isotherm models for phosphate removal using Zinc-doped biochar. [Condition: Adsorbent dosage 3 g/L; pH 5; Shaking speed 200 rpm; Operating time 2 h; Room temperature].

pyrolysis of metal chloride ($ZnCl_2$) and biomass feedstock. Impregnation of metal ions in biochar could increase the phosphate adsorption capacity of biochar due to good phosphate affinity to the metal oxide (ZnO), which was transformed from $ZnCl_2$ during the pyrolytic process (Wang et al., 2021). To enhance the credibility of the research, a comparison of the phosphate sorption capacities of biochar modified with zinc and other metals was presented in Table S1. The data demonstrated that the sorption performance of biochar studied in this research is highly comparable to other similar adsorbents. Moreover, the substantial sorption capacity suggests that P-laden ZBC could be utilized as a phosphorus fertilizer. The use of P-laden biochar is discussed in greater detail in Sections 3.6 and 3.7.

3.5. XPS study of P-laden ZBC

The XPS analysis of ZBC after phosphorus is shown in Fig. 5. The survey scan shows the existence of Zn, O, C, N, and P (Fig. 5 (a)), which additionally shows the Zn $2p_{3/2}$ peak at 1023.4 eV, which can be assigned to be $ZnO.ZnCl_2{\cdot}2H_2O$ The deconvoluted C1s narrow scan shown in Fig. S2 (b) shows that the C-C or C═C (π-π* interactions) at

Table 2
Calculated parameters of different sorption isotherm models.

Model	Langmuir				Freundlich				Temkin			
Parameter	q_m (mg/g)	k_L (L/mg)	R^2	MAPE	$k_F \left(\frac{mg\left(\frac{1}{1-\frac{1}{n}}\right)}{g} \bullet L^{\frac{1}{n}}\right)$	$1/n$	R^2	MAPE	b_T (J/mol)	k_T (L/mg)	R^2	MAPE
Value	42.41	1.87	0.89	8.91	27.33	0.11	0.97	4.49	3.82	27.26	0.96	5.53

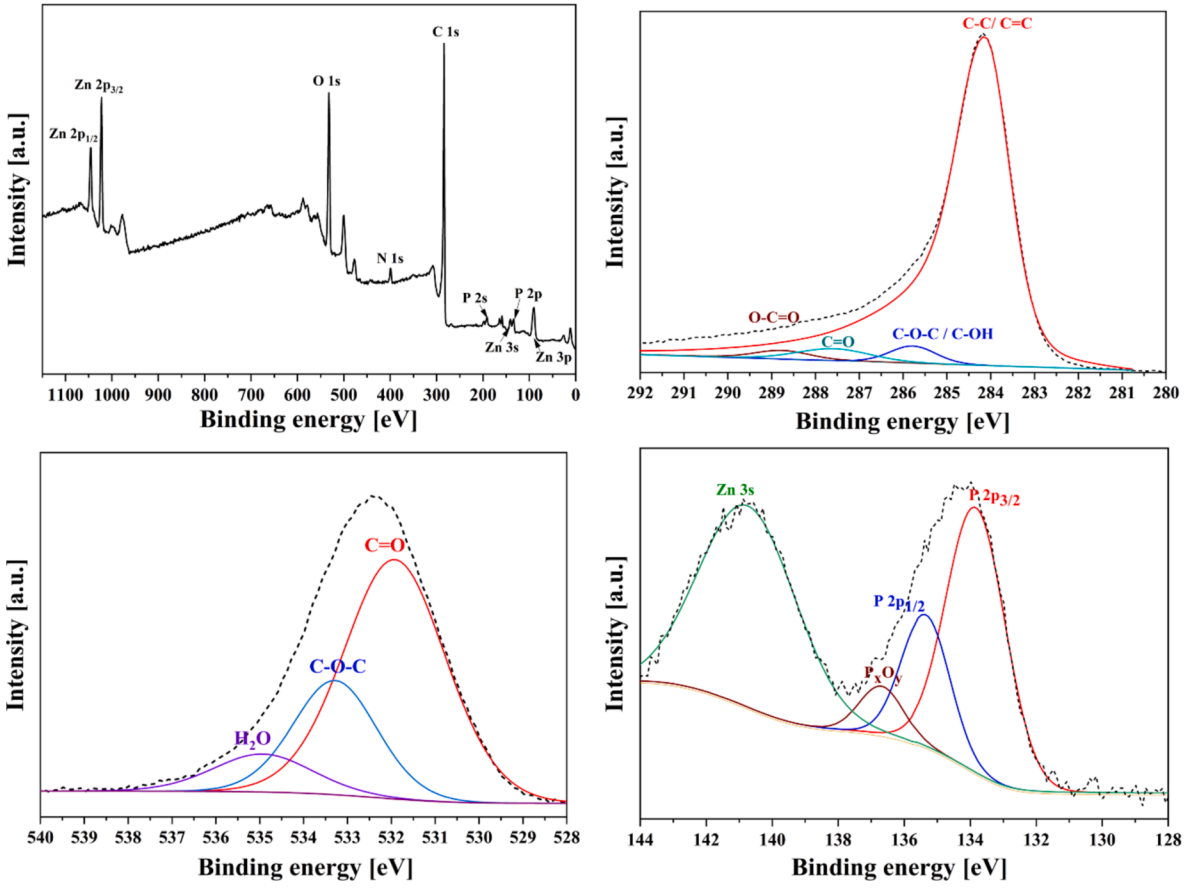

Fig. 5. XPS analysis of P-laden ZBC: (a) Overall survey scan, narrow (b) O, (c) C, and (d) P scan.

284.2 eV are the dominating bond formation for carbon. The other peaks at 285.8, 287.6, and 288.8 eV represent the C-O-C, C═O, and O-C═O bonds/functional groups, respectively. The O1s narrow scan (Fig. 5 (c)) confirms the existence of C═O (at 531.8 eV) and C-O-C (533.6 eV) bonds/functional group. In Fig. 5 (d), the deconvoluted P 2p narrow scan shows three peaks, which were at 133.8 eV, 135.3 eV, and 136.7 eV can be assigned to P $2p_{3/2}$, P $2p_{1/2}$, and P_xO_y /H_3PO_4 physisorbed in the surface. The P $2p_{3/2}$ peak at 133.8 eV position further illustrates the existence of PO_4^{3-} in interaction with zinc on the surface of the adsorbent (Navarathna et al., 2022). XPS analysis of ZBC before phosphate adsorption was given in Fig. S3.

The XRD analysis (in section 3.1) also confirmed the existence of both ZnO and $ZnO.ZnCl_2{\cdot}H_2O$ phases on the surface of ZBC, which was generated during low temperature (450 °C) pyrolysis process. The high phosphate uptake of ZBC can be associated with the existing form of zinc in the biochar surface.

3.6. Slow-release of phosphate from P-laden ZBC

The release of P from P-laden biochar was carried out by mixing deionized water without stirring. In several beakers, 200 mg of P-laden ZBC was poured into 100 ml of deionized water and left for the required time. The phosphate concentration was measured by centrifugation after separating the solid biochar from the solution. The study of phosphate release from P-laden ZBC is presented in Fig. 6, where it is evident that a slow release of phosphate occurs. Fig. 6 shows that the initial stage of phosphate release took up to 30 h, which was due to the strong adsorption bond of phosphate with the biochar surface. A faster rate was observed until the phosphate release reached 40 % of the adsorbed phosphate in 180 h (7.5 days), equivalent to approximately 17 mg-P/g of ZBC (17,000 mg-P/kg of ZBC). Afterward, the release rate slowed, and 42 % of total adsorbed P was released at 336 h, possibly due to the firmly attached phosphate in the biochar surface. The phosphate release rate in this study is significantly better than that of MgPA-BC (1 % with DI water) and CaPA-BC (1 % with DI water) (Jetsrisuparb et al., 2022). The SEM and EDS of 14-day slow-release P-laden ZBC biochar are shown in Fig. S1 and S4. The SEM image shows a relatively smooth surface of ZBC compared to pristine ZBC biochar, and EDS shows the presence of phosphorous remained after 14 days. A comparative FT-IR analysis between pristine, ZBC P-laden ZBC and after 14-days slow-release P-laden ZBC biochar is demonstrated in Fig. S5. A peak at 1098 cm-1 is visible for both P-laden biochars, which distinguish the phosphate band (Luna-Zaragoza et al., 2009). However, the intensity decreases for 14-day slow-released ZBC biochar compared to P-laden ZBC biochar.

The released amount of P is vital as the optimum P amount needed in soil (45–50 mg-P/kg soil) for plant growth and crop yields (Yao et al., 2013). Notably, among the total P in phosphate-laden biochar, about 19 % of the total P in phosphate-laden biochar could be termed as easily accessible P for plant (Yao et al., 2013). Therefore, the present study suggested a high feasibility of utilizing P-laden ZBC directly into the soil as a slow-release fertilizer for the sustainable production of crops. Since the biochar was derived from kitchen waste (vegetable and fruit) and is used for phosphate uptake, which could be utilized as a slow-release P-fertilizer, the developed system would be closer to attaining a circular economy.

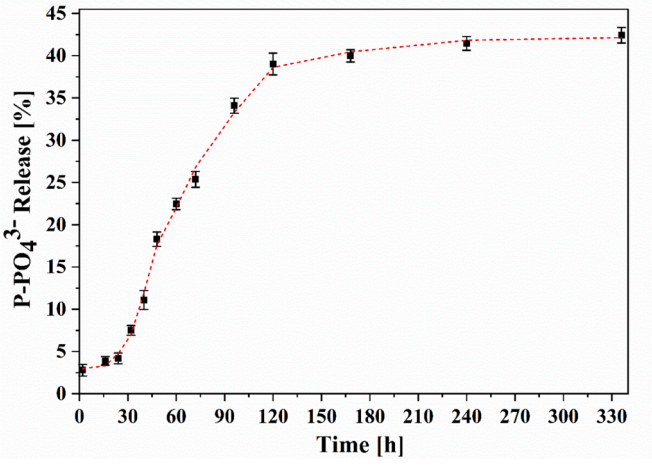

Fig. 6. Slow release of phosphate from P-laden ZBC. [Condition: 100 ml deionized water, 200 mg biochar].

3.7. Effectivity analysis of P-laden ZBC as a potential slow-release fertilizer

A study of the mung plant was conducted to analyze the effectiveness of the P-laden ZBC as a potential slow-release fertilizer. Three categorized pots control (without TSP and P-laden biochar), TSP fertilizer, and P-laden biochar were prepared. Ten mung seeds were planted in each category of pots. Within five days of seeding, 100 % germination was observed in the case of both control and TSP fertilized pots, where 90 % germination was observed for P-laden biochar. The low germination may be due to a subtle variation in seed quality. After 35 days, the average height of the mung plants in the pot mixed with P-laden biochar (P-ZBC with soil) was 30.10 cm, compared to 27.50 cm in the TSP-mixed pot and 28.90 cm in the soil-only pot. This clearly demonstrates a significant increase in plant height in the P-laden biochar treatment (P-ZBC with soil) compared to the TSP-mixed soil and the soil-only treatments. Similar results were observed in the growth of pepper seedlings using a phosphorus slow-release fertilizer (An et al., 2021). The plant growth data suggests that the release of phosphorus from traditional chemical fertilizers like TSP, which provides readily available phosphorus due to its high water solubility, is less effective than the superior slow-release capability of P-laden biochar. However, the dried biomass of the mung plant, measured after washing the whole plant with water and drying overnight at 80 °C, was found to be 66 mg, 53 mg, and 60 mg for P-laden biochar, TSP, and control-based plants, respectively.

After 70 days, the pods of mung plants from each type of pot were collected. It was found that 3.68 g, 3.14 g, and 2.86 g of mass per 100 mung beans yielded for P-laden biochar, TSP, and control-based plants, respectively. This finding indicates that the external phosphorus supply as a nutrient benefits mung cultivation. It further verifies that slow-release properties of P-laden biochar offer a better supply of phosphorus and are more efficient. Moreover, the dried biomass was measured again and was found to be 378 mg, 321 mg, and 267 mg for P-laden biochar, TSP, and control-based plants, respectively. Dry weight for mung plant followed an order of P-ZBC with soil > TSP-mixed soil > Soil-only. This suggests that P-laden biochar can improve mung plant production more effectively than traditional fertilizers (e.g., TSP) and soil. The results of the plant-based study are summarized in Table 3.

4. Conclusion

In this study, non-edible vegetable waste, a lignocellulosic material, was transformed into functional biochar through a co-pyrolysis method using magnesium and zinc chloride salts. The resulting biochar was

Table 3
Summarized results of the plant-based study.

Category	After 35 days		After 70 days	
	Plant height (cm)	Dry biomass (mg)	100 Bean weight (g)	Dry biomass (mg)
Control	28.90	60	2.86	267
TSP	27.50	53	3.14	321
P-laden ZBC	30.10	66	3.68	378

tested as an adsorbent for phosphate (P-PO_4^{3-}) from synthetic solutions. Results indicated that zinc chloride-doped biochar (ZBC) outperformed both pristine and magnesium chloride-doped biochar in phosphorus removal. The ZBC exhibited an adsorption capacity of 47.83 mg/g at pH five and followed pseudo-second-order kinetics, with sorption data aligning well with the Freundlich isotherm model. Additionally, P-laden ZBC demonstrated a slow release of phosphorus, with 42 % of the adsorbed phosphorus released over 336 h, highlighting its potential as a slow-release phosphorus fertilizer. A pot study using mung plants revealed that those grown with ZBC-enriched soil exhibited enhanced growth and produced higher dry biomass compared to plants grown with the other two categories. Notably, the weight of mung beans cultivated in ZBC-based pots was 17 % greater than that of those grown with triple super phosphate (TSP). These findings suggest that ZBC, derived from non-edible waste, can effectively recover phosphorus from wastewater and serve as a slow-release fertilizer in agricultural settings. The abundant availability of non-edible vegetable waste and the conversion process into biochar underline its potential role in promoting a circular economy.

CRediT authorship contribution statement

Rajesh Chanda: Writing – review & editing, Writing – original draft, Supervision, Project administration, Methodology, Conceptualization. **Toslim Jahid:** Resources, Investigation, Formal analysis. **Anik Karmokar:** Resources, Investigation. **Bejoy Hossain:** Resources, Investigation. **Md. Moktadir:** Resources, Investigation. **Md. Saiful Islam:** Writing – review & editing, Validation, Software. **Nirupam Aich:** Writing – review & editing, Writing – original draft, Project administration. **Biplob Kumar Biswas:** Writing – review & editing, Writing – original draft, Project administration, Funding acquisition.

Declaration of competing interest

The authors declare that they have no known competing financial interests or personal relationships that could have appeared to influence the work reported in this paper.

Acknowledgments

This work was financially supported by the Ministry of Science and Technology, Government of the People's Republic of Bangladesh of Bangladesh (Grant number: SRG-232394, Fiscal year: 2023-24).

Appendix A. Supplementary data

Supplementary data to this article can be found online at https://doi.org/10.1016/j.clema.2024.100287.

Data availability

Data will be made available on request.

References

Alemu, A., Lemma, B., Gabbiye, N., 2019. Adsorption of chromium (III) from aqueous solution using vesicular basalt rock. Cogent Environ. Sci. 5, 1650416. https://doi.org/10.1080/23311843.2019.1650416.

An, X., Wu, Z., Liu, X., Shi, W., Tian, F., Yu, B., 2021. A new class of biochar-based slow-release phosphorus fertilizers with high water retention based on integrated co-pyrolysis and co-polymerization. Chemosphere 285, 131481. https://doi.org/10.1016/j.chemosphere.2021.131481.

Argus Consulting Services, 2023. Phosphate rock Resources & Reserves 566.

Ayawei, N., Ebelegi, A.N., Wankasi, D., 2017. Modelling and interpretation of adsorption isotherms. J. Chem. 2017, 1–11. https://doi.org/10.1155/2017/3039817.

Capanoglu, E., Nemli, E., Tomas-Barberan, F., 2022. Novel approaches in the valorization of agricultural wastes and their applications. J. Agric. Food Chem. 70, 6787–6804. https://doi.org/10.1021/acs.jafc.1c07104.

Chanda, R., Islam, M.S., Biswas, B.K., 2023. N and P removal from wastewater using rice husk ash-derived silica-based Fe-ZSM-5 zeolite. Clean. Eng. Technol. 16, 100675. https://doi.org/10.1016/j.clet.2023.100675.

Chanda, R.K., Jahid, T., Hassan, M.N., Yeasmin, T., Biswas, B.K., 2024. Cauliflower stem-derived biochar for effective adsorption and reduction of hexavalent chromium in synthetic wastewater: A sustainable approach. Environ. Adv. 15, 100458. https://doi.org/10.1016/j.envadv.2023.100458.

Chen, S.S., Cao, Y., Tsang, D.C.W., Tessonnier, J.-P., Shang, J., Hou, D., Shen, Z., Zhang, S., Ok, Y.S., Wu, K.-C.-W., 2020. Effective dispersion of MgO nanostructure on biochar support as a basic catalyst for glucose isomerization. ACS Sustain. Chem. Eng. 8, 6990–7001. https://doi.org/10.1021/acssuschemeng.0c00278.

Chen, R.-F., Liu, T., Rong, H.-W., Zhong, H.-T., Wei, C.-H., 2021. Effect of organic substances on nutrients recovery by struvite electrochemical precipitation from synthetic anaerobically treated swine wastewater. Membranes (basel). 11, 594. https://doi.org/10.3390/membranes11080594.

Christensen, M.L., Cvitanich, C., Quist-Jensen, C.A., Thau, M., Malmgren-Hansen, B., 2022. Precipitation and recovery of phosphorus from the wastewater hydrolysis tank. Sci. Total Environ. 813, 151875. https://doi.org/10.1016/j.scitotenv.2021.151875.

Commission, E., 2023. Circular economy – New tool for measuring progress. Publications Office of the European Union. https://doi.org/doi/10.2779/1618.

Dhaliwal, S.S., Sharma, V., Shukla, A.K., Kaur, M., Kaur, J., Verma, V., Singh, P., Barek, V., Gaber, A., Hossain, A., 2023. Biofortification of mungbean (Vigna radiata L. (Wilczek)) with boron, zinc and iron alters its grain yield and nutrition. Sci. Rep. 13, 3506. https://doi.org/10.1038/s41598-023-30539-6.

Feng, D., Wang, S., Zhang, Y., Zhao, Y., Sun, S., Chang, G., Lai, X., Tan, H., Qin, Y., 2020. Review of carbon fixation evaluation and emission reduction effectiveness for biochar in China. Energy & Fuels 34, 10583–10606. https://doi.org/10.1021/acs.energyfuels.0c02396.

Ghosh, S., Lobanov, S., Lo, V.K., 2019. An overview of technologies to recover phosphorus as struvite from wastewater: advantages and shortcomings. Environ. Sci. Pollut. Res. 26, 19063–19077. https://doi.org/10.1007/s11356-019-05378-6.

Hale, S.E., Alling, V., Martinsen, V., Mulder, J., Breedveld, G.D., Cornelissen, G., 2013. The sorption and desorption of phosphate-P, ammonium-N and nitrate-N in cacao shell and corn cob biochars. Chemosphere 91, 1612–1619. https://doi.org/10.1016/j.chemosphere.2012.12.057.

He, X., Zhang, T., Ren, H., Li, G., Ding, L., Pawlowski, L., 2017. Phosphorus recovery from biogas slurry by ultrasound/H2O2 digestion coupled with HFO/biochar adsorption process. Waste Manag. 60, 219–229. https://doi.org/10.1016/j.wasman.2016.08.032.

Jellali, S., Hadroug, S., Al-Wardy, M., Al-Nadabi, H., Nassr, N., Jeguirim, M., 2023. Recent developments in metallic-nanoparticles-loaded biochars synthesis and use for phosphorus recovery from aqueous solutions. A critical review. J. Environ. Manage. 342, 118307. https://doi.org/10.1016/j.jenvman.2023.118307.

Jellali, S., Khiari, B., Al-Balushi, M., Al-Sabahi, J., Hamdi, H., Bengharez, Z., Al-Abri, M., Al-Nadabi, H., Jeguirim, M., 2024. Use of waste marble powder for the synthesis of novel calcium-rich biochar: Characterization and application for phosphorus recovery in continuous stirring tank reactors. J. Environ. Manage. 351, 119926. https://doi.org/10.1016/j.jenvman.2023.119926.

Jetsrisuparb, K., Jeejaila, T., Saengthip, C., Kasemsiri, P., Ngernyen, Y., Chindaprasirt, P., Knijnenburg, J.T.N., 2022. Tailoring the phosphorus release from biochar-based fertilizers: role of magnesium or calcium addition during co-pyrolysis. RSC Adv. 12, 30539–30548. https://doi.org/10.1039/D2RA05848K.

Jin, X., Guo, J., Hossain, M.F., Lu, J., Lu, Q., Zhou, Y.i., Zhou, Y., 2024. Recent advances in the removal and recovery of phosphorus from aqueous solution by metal-based adsorbents: A review. Resour. Conserv. Recycl. 204, 107464. https://doi.org/10.1016/j.resconrec.2024.107464.

Jones, F., Tran, H., Lindberg, D., Zhao, L., Hupa, M., 2013. Thermal stability of zinc compounds. Energy & Fuels 27, 5663–5669. https://doi.org/10.1021/ef400505u.

Jupp, A.R., Beijer, S., Narain, G.C., Schipper, W., Slootweg, J.C., 2021. Phosphorus recovery and recycling – closing the loop. Chem. Soc. Rev. 50, 87–101. https://doi.org/10.1039/D0CS01150A.

Kamusoko, R., Jingura, R.M., Parawira, W., Chikwambi, Z., 2021. Strategies for valorization of crop residues into biofuels and other value-added products. Biofuels. Bioprod. Biorefining 15, 1950–1964. https://doi.org/10.1002/bbb.2282.

Khandaker, S., Kuba, T., Kamida, S., Uchikawa, Y., 2017. Adsorption of cesium from aqueous solution by raw and concentrated nitric acid–modified bamboo charcoal. J. Environ. Chem. Eng. 5, 1456–1464. https://doi.org/10.1016/j.jece.2017.02.014.

Kizito, S., Luo, H., Wu, S., Ajmal, Z., Lv, T., Dong, R., 2017. Phosphate recovery from liquid fraction of anaerobic digestate using four slow pyrolyzed biochars: Dynamics of adsorption, desorption and regeneration. J. Environ. Manage. 201, 260–267. https://doi.org/10.1016/j.jenvman.2017.06.057.

Kumar, P., Sudha, S., Chand, S., Srivastava, V.C., 2010. Phosphate removal from aqueous solution using coir-pith activated carbon. Sep. Sci. Technol. 45, 1463–1470. https://doi.org/10.1080/01496395.2010.485604.

Li, X., Shen, S., Xu, Y., Guo, T., Dai, H., Lu, X., 2021. Application of membrane separation processes in phosphorus recovery: a review. Sci. Total Environ. 767, 144346. https://doi.org/10.1016/j.scitotenv.2020.144346.

Li, R., Wang, J.J., Zhang, Z., Awasthi, M.K., Du, D., Dang, P., Huang, Q., Zhang, Y., Wang, L., 2018. Recovery of phosphate and dissolved organic matter from aqueous solution using a novel CaO-MgO hybrid carbon composite and its feasibility in phosphorus recycling. Sci. Total Environ. 642, 526–536. https://doi.org/10.1016/j.scitotenv.2018.06.092.

Lin, H., Wang, Y., Dong, Y., 2024. A review of methods, influencing factors and mechanisms for phosphorus recovery from sewage and sludge from municipal

wastewater treatment plants. J. Environ. Chem. Eng. 12, 111657. https://doi.org/10.1016/j.jece.2023.111657.

Luna-Zaragoza, D., Romero-Guzmán, E.T., Reyes-Gutiérrez, L.R., 2009. Surface and physicochemical characterization of phosphates vivianite, $Fe_2(PO_4)_3$ and hydroxyapatite, Ca_5. J. Miner. Mater. Charact. Eng. 08, 591–609. https://doi.org/10.4236/jmmce.2009.88052.

Moezzi, A., Cortie, M., McDonagh, A., 2016. Transformation of zinc hydroxide chloride monohydrate to crystalline zinc oxide. Dalt. Trans. 45, 7385–7390. https://doi.org/10.1039/C5DT04864H.

Navarathna, C.M., Pennisson, J.E., Dewage, N.B., Reid, C., Dotse, C., Jazi, M.E., Rodrigo, P.M., Zhang, X., Farmer, E., Watson, C., Craig, D.O., Ramirez, A., Walker, M., Madduri, S., Mohan, D., Mlsna, T.E., 2022. Adsorption of phosphates onto Mg/Al-oxide/hydroxide/sulfate-impregnated douglas fir biochar. Processes 11, 111. https://doi.org/10.3390/pr11010111.

Pal, D.B., Singh, A., Jha, J.M., Srivastava, N., Hashem, A., Alakeel, M.A., Abd_Allah, E.F., Gupta, V.K., 2021. Low-cost biochar adsorbents prepared from date and delonix regia seeds for heavy metal sorption. Bioresour. Technol. 339, 125606. https://doi.org/10.1016/j.biortech.2021.125606.

Phuong Tran, T.C., Nguyen, T.P., Nguyen Nguyen, T.T., Thao Tran, T.N., Hang Nguyen, T.A., Tran, Q.B., Nguyen, X.C., 2021. Enhancement of phosphate adsorption by chemically modified biochars derived from Mimosa pigra invasive plant. Case Stud. Chem. Environ. Eng. 4, 100117. https://doi.org/10.1016/j.cscee.2021.100117.

Samaraweera, H., Palansooriya, K.N., Dissanayake, P.D., Khan, A.H., Sillanpää, M., Mlsna, T., 2023. Sustainable phosphate removal using Mg/Ca-modified biochar hybrids: Current trends and future outlooks. Case Stud. Chem. Environ. Eng. 8, 100528. https://doi.org/10.1016/j.cscee.2023.100528.

Santos, A.F., Almeida, P.V., Alvarenga, P., Gando-Ferreira, L.M., Quina, M.J., 2021. From wastewater to fertilizer products: alternative paths to mitigate phosphorus demand in European countries. Chemosphere 284, 131258. https://doi.org/10.1016/j.chemosphere.2021.131258.

Sinha, R., Kumar, R., Sharma, P., Kant, N., Shang, J., Aminabhavi, T.M., 2022. Removal of hexavalent chromium via biochar-based adsorbents: State-of-the-art, challenges, and future perspectives. J. Environ. Manage. 317, 115356. https://doi.org/10.1016/j.jenvman.2022.115356.

Sun, X., Atiyeh, H.K., Li, M., Chen, Y., 2020. Biochar facilitated bioprocessing and biorefinery for productions of biofuel and chemicals: A review. Bioresour. Technol. 295, 122252. https://doi.org/10.1016/j.biortech.2019.122252.

Wang, P., Zhi, M., Cui, G., Chu, Z., Wang, S., 2021. A comparative study on phosphate removal from water using Phragmites australis biochars loaded with different metal oxides. R. Soc. Open Sci. 8, 201789. https://doi.org/10.1098/rsos.201789.

Weferling, N., Zhang, S.M., Chiang, C.H., 2016. Commercial organophosphorus chemicals: status and new developments. Procedia Eng. 138, 291–301. https://doi.org/10.1016/j.proeng.2016.02.087.

Witek-Krowiak, A., Gorazda, K., Szopa, D., Trzaska, K., Moustakas, K., Chojnacka, K., 2022. Phosphorus recovery from wastewater and bio-based waste: an overview. Bioengineered 13, 13474–13506. https://doi.org/10.1080/21655979.2022.2077894.

Yang, H., Ye, S., Zeng, Z., Zeng, G., Tan, X., Xiao, R., Wang, J., Song, B., Du, L., Qin, M., Yang, Y., Xu, F., 2020. Utilization of biochar for resource recovery from water: A review. Chem. Eng. J. 397, 125502. https://doi.org/10.1016/j.cej.2020.125502.

Yao, Y., Gao, B., Chen, J., Yang, L., 2013. Engineered biochar reclaiming phosphate from aqueous solutions: mechanisms and potential application as a slow-release fertilizer. Environ. Sci. Technol. 47, 8700–8708. https://doi.org/10.1021/es4012977.

Yu, J., Hu, H., Wu, X., Zhou, T., Liu, Y., Ruan, R., Zheng, H., 2020. Coupling of biochar-mediated absorption and algal-bacterial system to enhance nutrients recovery from swine wastewater. Sci. Total Environ. 701, 134935. https://doi.org/10.1016/j.scitotenv.2019.134935.

Zeng, L., Li, X., Liu, J., 2004. Adsorptive removal of phosphate from aqueous solutions using iron oxide tailings. Water Res. 38, 1318–1326. https://doi.org/10.1016/j.watres.2003.12.009.

Zhang, H., Cao, T., Cheng, Y., 2014. Synthesis of nanostructured MgO powders with photoluminescence by plasma-intensified pyrohydrolysis process of bischofite from brine. Green Process. Synth. 3, 215–222. https://doi.org/10.1515/gps-2014-0026.

Zhang, H., Wei, Z., Xiong, D., Wu, Y., Tong, M., Su, H., Zhang, Z., Liao, J., 2024. Investigation into the structure and properties of biochar co-activated by ZnCl2 and NaHCO3 under low temperature conditions. Materials (basel) 17, 942. https://doi.org/10.3390/ma17040942.